Journal of Thermal Science Vol.33, No.5 (2024) 1946−1960

https://doi.org/10.1007/s11630-024-1993-1 **Article ID: 1003-2169(2024)05-1946-15**

Comprehensive Assessment of STGSA Generated Skeletal Mechanism for the Application in Flame-Wall Interaction and Flame-Flow Interaction

YU Chunkan[1*], YANG Bin[2]

1. Institute of Technical Thermodynamics, Karlsruhe Institute of Technology, Karlsruhe 76131, Germany
2. Center for Combustion Energy, Tsinghua University, Beijing 100084, China

Abstract: In this study, we conduct a thorough evaluation of the STGSA-generated skeletal mechanism for C_2H_4/air. Two STGSA-reduced mechanisms are taken into account, incorporating basic combustion models such as the homogeneous reactor model, one-dimensional flat premixed flame, and non-premixed counterflow flame. Subsequently, these models are applied to more complex combustion systems, considering factors like flame-flow interaction and flame-wall interaction. These considerations take into account additional physical parameters and processes such as mixing frequency and quenching. The results indicate that the skeletal mechanism adeptly captures the behavior of these complex combustion systems. However, it is suggested to incorporate strain rate considerations in generating the skeletal mechanism, especially when the combustion system operates under high turbulent intensity.

Keywords: Species-Targeted Global Sensitivity Analysis (STGSA); mechanism reduction; Partially Stirred Reactor (PaSR); spark ignition; Head-on Quenching (HoQ)

1. Introduction

Detailed chemical kinetics involves a large number of species, and each considered reactive species results in a governing equation for that species [1–4]. Even for the smallest hydrocarbon species CH_4, it involves more than 30 reactive species [5], which means that more than 30 governing equations for reactive species must be numerically integrated simultaneously. Furthermore, the reaction rate constants for all elementary reactions are described by the Arrhenius law, which exhibits a high degree of nonlinearity and stiffness [1–3]. Both issues lead to the fact that the use of detailed chemistry in the simulation of reactive flames is highly computationally expensive, and its use is still restricted to simple combustion configurations (e.g., homogeneous reactors or laminar flame) and geometries. Even with the use of high-performance computing (HPC), the application of Direct Numerical Simulation (DNS) or Large Eddy Simulation (LES) methods for turbulent reactive flames is still limited to small molecular fuels such as hydrogen, ammonia, or methane [6–10]. For heavy molecular fuels, the corresponding reduced chemical mechanisms must be used to allow DNS or LES simulation [11–15].

Therefore, model reduction for chemical kinetics involves the process of simplifying complex chemical reaction mechanisms while retaining essential information. One common approach for simplifying chemical kinetics is manifold-based simplified chemistry, in which all thermo-kinetic states (e.g., temperature,

Received: Jan 20, 2024
AE: CHEN Zheng

Corresponding author: YU Chunkan E-mail: chunkan.yu@kit.edu

enthalpy, pressures, and species concentrations) are tabulated as functions of progress variables [1]. Some important candidates for this group include the intrinsic low-dimensional manifold (ILDM) [16], flamelet/ progress variable (PV) method [17, 18], flame-prolongation of ILDM (FPI) [19], and reaction-diffusion manifolds (REDIM) [20]. Although, for manifold-based simplified chemistry, all species are retained, the corresponding reduced schema can- not be written in the form of conventional chemical reactions, and the application of these reduced kinetics requires solving governing equations for progress variables, which cannot be directly used in many commercial software.

Another common approach is to construct global reactions [21] or virtual reactions [22], aiming to capture desired flame parameters such as flame speed, flame temperature, concentrations of certain species, and so on. The third common approach is to generate the skeletal mechanism, which involves identifying and eliminating negligible species or reactions that have a minimal impact on the overall system behavior. Some important possible methods include sensitivity analysis [2], computational singular perturbation (CSP) [23], directed relation graph (DRG) and its variation [24–27], and species-targeted sensitivity analysis (STSA) [28]. Although, in all techniques for skeletal mechanism generation, some species are removed from the original species lists, the resulting skeletal mechanism still contains elementary reactions, which can be directly used for other purposes without modifying the numerical implementation.

Despite the ease of usage of skeletal mechanisms, the resulting reduced chemical kinetics usually still involve more than 20 species, even though the number of species from the original detailed chemical mechanisms is higher. For instance, a 39-species skeletal mechanism for DME is generated based on the DRG method from a 55-species detailed chemistry to enable DNS simulation [29]. Additionally, a 115-species skeletal mechanism for toluene reference fuel is generated based on the STSA method from a 451-species detailed chemistry to accurately capture laminar flame speed and NO_x emission [28]. In this context, to generate a skeletal mechanism with less computational cost, its validity typically aims at capturing ignition delay time (IDT), laminar flame speeds, and species concentrations based on simple combustion systems such as homogeneous reactors, perfectly stirred reactors, and laminar premixed flames [24–27]. If these quantities are well reproduced by the skeletal mechanisms, it is assumed that they are also suitable for more complex systems, such as turbulent reacting flames [29, 30]. To the author's knowledge, there is limited literature reporting the validation of skeletal mechanisms for complex systems through comparison with detailed chemical mechanisms. In Ref. [31], a skeletal mechanism was generated and validated for large-scale direct numerical simulations of lean turbulent premixed flames, directly showcasing the performance of the skeletal mechanism for use in turbulent premixed flames. However, direct comparisons between skeletal mechanisms and detailed chemical mechanisms are challenging for complex combustion systems, as numerical simulations based on detailed chemical mechanisms, involving a large number of reactive species, are computationally expensive.

Nevertheless, real combustion systems in practical applications are much more complicated, involving processes such as forced spark ignition, transient quenching if the flame approaches or nears the wall, strong interactions between the flame and turbulence, and additional physical parameters that significantly influence flame behaviors [14, 32, 33]. Therefore, the purpose of this work is to provide a comprehensive assessment of a skeletal mechanism that has only been validated for simple combustion models (e.g., ignition delay time in homogeneous reactors, laminar flame speed in one-dimensional flat premixed flames, and extinction limits for one-dimensional counterflow diffusion flames). The skeletal mechanisms will be tested for more complex but still computationally inexpensive combustion systems to check their validity. A comprehensive assessment will include:

(1) Flame-Flow Interaction: Stochastic modeling for Partially Stirred Reactor (PaSR),

(2) Flame-Flow Interaction: Spark ignition in strained premixed flame,

(3) Flame-Wall Interaction: Head-on Quenching (HoQ) process of laminar premixed flame.

2. Mechanism Reduction: Species-Targeted Global Sensitivity Analysis (STGSA)

The main idea of the STGSA concept is that, even with the inclusion of uncertainties in the chemical reaction rates, the STGSA method can still identify coupling species and measure the importance of species for the considered configuration. In this case, STGSA can identify global redundant species under uncertainties in the reaction rates, while DRG-based methods are very sensitive to uncertainties in the reaction rates. It is shown for both ethylene/air and n-heptane/air combustion reactions in Ref. [34] that the STGSA can generate skeletal mechanisms with the smallest number of species compared with DRG-based methods, while maintaining high accuracy.

Given that the focus of this work is not on the methodology of STGSA itself but rather on the validation of the STGSA-generated skeletal mechanism for more

complex combustion systems, we will briefly mention some important properties and advantages of STGSA, along with its validation for standard combustion models. For more detailed information regarding the methodology and implementation, readers can refer to Ref. [34].

2.1 STGSA skeletal mechanism for C_2H_4

In Ref. [34], a detailed C_2H_4 chemical mechanism with 111 species was reduced based on STGSA to a skeletal mechanism with 33 species, and during the generation procedure, the ignition delay time and the homogeneous reactor model were applied to evaluate the quality of reduced mechanism.

In Ref. [35], additional extinction strain rate (ESR) for the counterflow flame was considered during the generation procedure to qualify the reduced mechanism, and the resulted reduced mechanism includes 45 species.

Fig. 1 shows the convergence of error limit against the number of species, depending on different targets for validation. The square dashed line represents the case if only the ignition delay time (IDT) is considered as target quantity [34] and the resulted skeletal mechanism includes 33 sp (sk-33sp). The circle point line represents the case if the additional extinction strain rate (ESR) is considered as target quantity [35] and the corresponding skeletal mechanism includes 45 species (sk-45sp). It is observed that the error limit converges much faster if only the IDT is considered as target quantity.

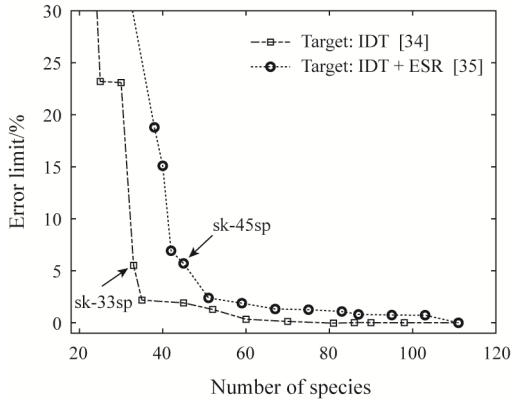

Fig. 1 Error limit as a function of number of species in the reduced mechanism. Square dashed line: considering IDT as target quantity; Circle dashed line: considering both IDT and ESR as target quantity.

To quantify the errors of skeletal mechanism for any quantity Q, we define the relative errors in absolute value as:

$$\text{Relative error}\ (\%) = \left|\frac{Q_{\text{skeletal}} - Q_{\text{detailed}}}{Q_{\text{detailed}}}\right| \times 100\% \quad (1)$$

Fig. 2 shows the comparison of laminar flame speed by using these two skeletal mechanisms, which shows again that by considering the extinction limit in the generation, the corresponding sk-45sp gives better prediction and the errors are all less than 3%. Note that the LBV can also be considered as target quantity. However, many studies (e.g. [26, 30, 34]) show that the consideration of IDT only is sufficient to reproduce the LBV with good accuracy. Therefore, in Ref. [34], only IDT is considered as target quantity.

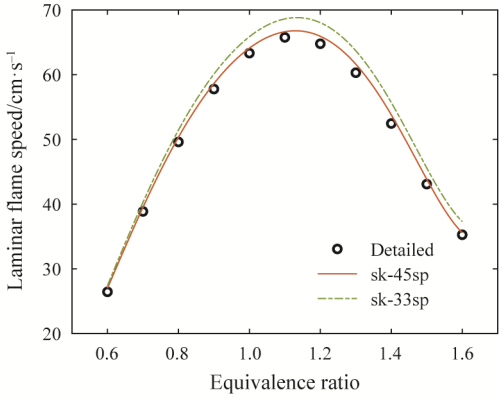

(a) Comparison of laminar burning velocity

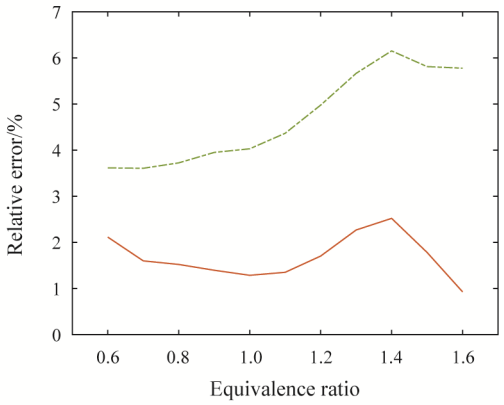

(b) Relative errors of two skeletal mechanisms

Fig. 2 Circles: detailed mechanism (circles); Solid lines: sk-45sp, the 45-species skeletal mechanism; Dashed lines: sk-33sp, the 33-species skeletal mechanism. The unburnt gas temperature: 300 K; Pressure: 101.325 kPa

2.2 Validation for PSR model

The Perfectly Stirred Reactor (PSR) model is one of the simplest models describing the chemical process of a homogeneous mixed gas mixture inside a reactor, and has been applied for various purposes in the CFD calculation [36–39]. Besides the chemical process, the PSR model also takes into account the residence time as physical parameter. It is assumed for the PSR model that the inlet gas mixture mixes infinitely fast with the gas mixture inside the reactor. The mathematical formulation follows the one from Ref. [40]:

$$\frac{\partial h}{\partial t} = -\frac{h - h_{\text{in}}}{\tau_{\text{res}}} \tag{2}$$

$$\frac{\partial p}{\partial t} = 0 \tag{3}$$

$$\frac{\partial Y_i}{\partial t} = -\frac{Y_i - Y_{i,\text{in}}}{\tau_{\text{res}}} + \frac{\dot{\omega}_i M_i}{\rho} \tag{4}$$

where h is the specific enthalpy; p the pressure; t the time and ρ the mixture density. For ith species, it has the mass fraction Y_i, molar mass M_i and molar formation rate $\dot{\omega}_i$. The subscript in stands for the thermo-kinetic state of the incoming flows.

In this PSR model, τ_{res} is the physical parameter and is often referred to residence time, describing the reactants flowing through the reactor and being the primary controlling the chemical processes. It is well known that a short residence time can cause flame extinction [41, 42], and it is of great interest to check, whether the generated skeletal mechanism can also predict such extinction behavior in the PSR model with good accuracy.

The dependence of temperature and species mole fractions at steady state on residence time are predicted by using detailed mechanism and two skeletal mechanisms, as shown in Fig. 3. In this figure, the unburnt gas is considered as mixture with three different fuel/air equivalent ratios with 300 K. All curves end at extinction residence time, below which no burning solution can be obtained at steady state. It is observed clearly that the results predicted by using both sk-45sp and sk-33sp mechanisms agree with detailed solution very good, and the sk-45sp results are slightly better than the sk-33sp results.

At long residence time in Fig. 3, the errors of skeletal mechanisms are negligibly small because they tend to be homogeneous reactor systems, and the skeletal mechanisms are generated based on considering the homogeneous reactor system in terms of IDT. At short residence time in Fig. 3, which are close to extinction, there is a strong interaction between physical time scales and chemical time scales. The strain rate describes how fast the flow velocity is. The higher the strain rate, the higher the flow velocity is, and the shorter the time the flow passes one position. By considering the ESR as the target quantity, the strain rate can be considered an additional characteristic physical time scale. If the ESR can be well-captured, then the thermo-kinetic quantities at short residence time can also be well-captured.

While the temperature and species concentrations against residence time are less critical in the PSR model, the extinction residence time is more critical and

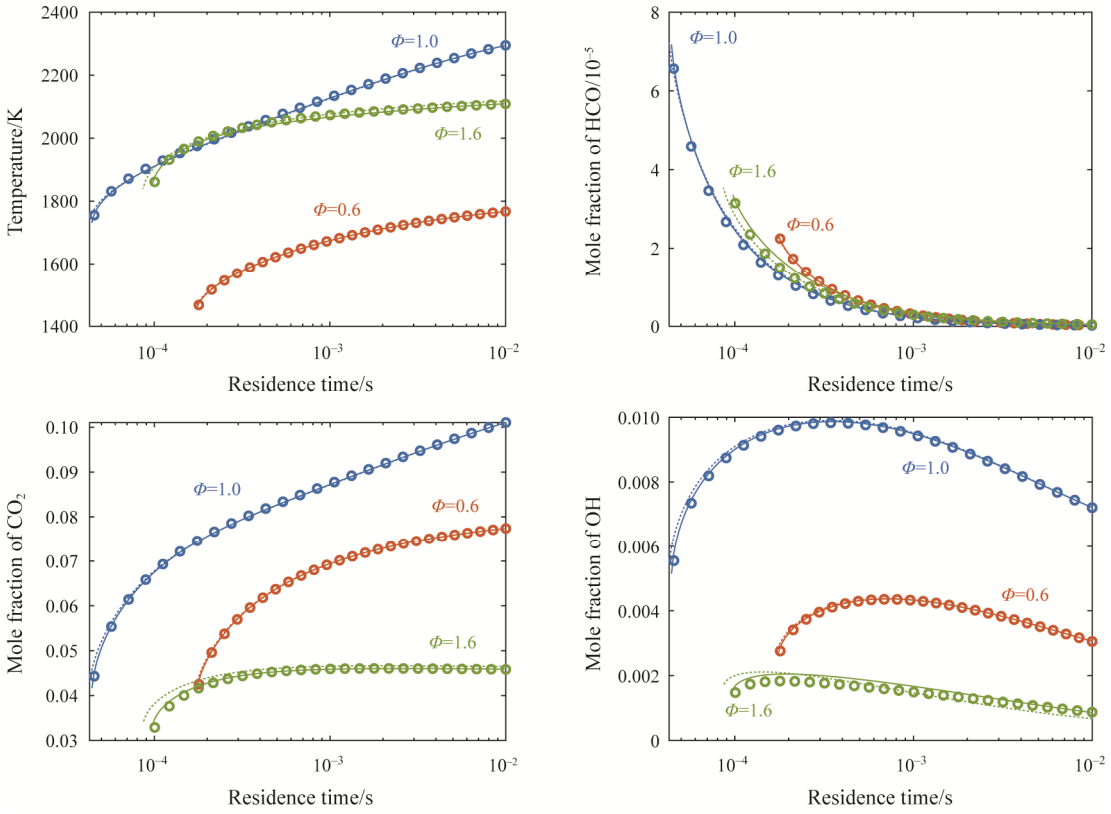

Fig. 3 Circles: detailed mechanism (circles); Solid lines: sk-45sp, the 45-species skeletal mechanism; Dashed lines: sk-33sp, the 33-species skeletal mechanism. Variation of fuel/air equivalence ratio: 0.6 (red), 1.0 (blue) and 1.6 (green). The unburnt gas temperature: 300 K; Pressure: 101.325 kPa

interesting, since this quantity reflects the interaction between the chemical kinetics and the physical parameter (e.g. residence time). Therefore, in Fig. 4 the extinction residence time against equivalent ratios are predicted by detailed and these two skeletal mechanisms. Meanwhile, the relative errors of both skeletal mechanisms are also presented. Similar to the observation from Fig. 2, the applied skeletal mechanisms can represent the extinction residence time with good accuracy, and the relative errors are below 10%. Furthermore, the sk-45sp results are better than the sk-33sp results.

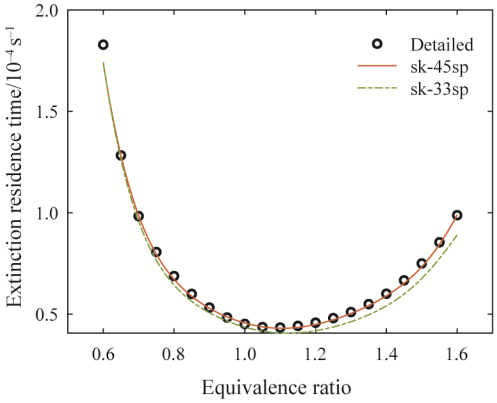

(a) Comparison of extinction residence time

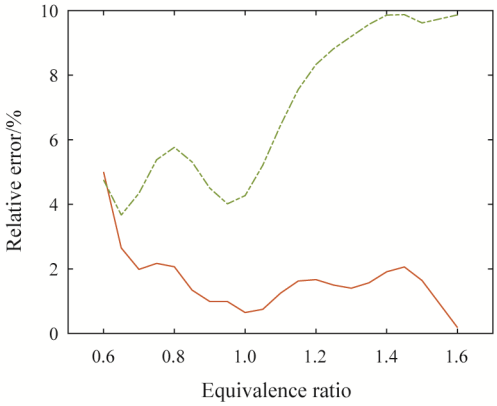

(b) Relative errors of two skeletal mechanisms

Fig. 4 Circles: detailed mechanism (circles); Solid lines: sk-45sp, the 45-species skeletal mechanism; Dashed lines: sk-33sp, the 33-species skeletal mechanism. The unburnt gas temperature: 300 K; Pressure: 101.325 kPa.

The conclusion in this section is consistent with those reported for various other fuels in other literature such as [25, 30, 43], namely the skeletal mechanisms generated by only considering the auto-ignition problems can also be applicable for PSR model with good accuracy.

3. Combustion Models for Validation

As discussed above, the generated skeletal mechanisms are usually validated against the ignition delay time and the laminar flame speed, and the resulted skeletal mechanisms will be applied for further more complex turbulent flame simulation [12, 44, 45]. In this section, we will introduce three more complex combustion systems, which are still computational achievable and can be used for validation of skeletal mechanisms without high computational cost.

3.1 Flame-flow interaction: Stochastic modeling for Partially Stirred Reactor (PaSR)

Although the skeletal mechanism generated by considering only the ignition delay time already gives accurate prediction for the PSR model, the rate of chemical processes in the PSR model is still controlled by chemical kinetic rates, as in the homogeneous reactor models. For the Partially Stirred Reactor (PaSR) model, which will be shortly introduced in this section, the inlet gas mixture and gas mixture inside the reactor are only partially mixed with each other and the mixing intensity is considered by mixing frequency as an additional physical parameter. Hence, the chemical process in the PaSR is mainly controlled by the degree of mixing, and the effect of mixing process on the chemistry can be evaluated [46–48]. With an additional advantage that the PaSR model can be expressed in simple ODE system, the PaSR model is easy but useful to investigate the turbulence-chemistry interaction [46, 47].

According to Refs. [46, 47], the PaSR can be modeled in a stochastic way, and the single-point joint scalar PDF can be used to determine the averaged values and the corresponding fluctuation of the thermo-kinetic states. Say the PDF is symbolized as $f_{\vec{\phi}}(\vec{\psi},t)$, the resulting joint PDF equation for the PaSR is [46]

$$\frac{\partial \tilde{f}_{\vec{\phi}}}{\partial t}=\frac{1}{\tau_{\mathrm{res}}}\left\{\tilde{f}_{\vec{\phi},\mathrm{inlet}}-f_{\vec{\phi}}\right\}-\sum_{\alpha=1}^{n_s+1}\frac{\partial}{\partial \psi_\alpha}\left\{R_\alpha(\vec{\psi})\cdot\tilde{f}_{\vec{\phi}}\right\}-\sum_{\alpha=1,\beta=1}^{n_s+2}\frac{\partial^2}{\partial\psi_\alpha\partial\psi_\beta}\left\{\left\langle\varepsilon_{\alpha\beta}\middle|\vec{\phi}=\vec{\psi}\right\rangle\tilde{f}_{\vec{\phi}}\right\} \tag{5}$$

where R_α is the source term of αth species in $\vec{\phi}$, and $\varepsilon_{\alpha\beta}$ the cross-scalar dissipation rate. Due to high computational cost if this transported PDF equation is directly solved, the Monte Carlo particle method is a more computational efficient way [49]. By using the Monte Carlo particle method, the $f_{\vec{\phi}}(\vec{\psi},t)$ is represented by N_p stochastic particles in thermokinetic state space such as $\vec{\psi}^{(k)}=\left(h^{(k)},p^{(k)},Y_i^{(k)}\right)^{\mathrm{T}}$ with k=1, 2, …, N_p.

A detailed numerical algorithm can be found in Refs. [46, 49]. However, it is worth mentioning here that the most important step in the numerical simulation is the mixing process which describes the cross-scalar dissipation rate in Eq. (5). In the present work, the mixing process is modeled by the Modified Curl's Model

(MCM) [50], in which the thermo-kinetic states of two randomly selected particle (denoted by p and q) after mixing processes are

$$\begin{aligned}\vec{\psi}_{\text{new}}^{(p)} &= \vec{\psi}^{(p)} + \frac{1}{2}\mu\left(\vec{\psi}^{(q)} - \vec{\psi}^{(p)}\right)\\ \vec{\psi}_{\text{new}}^{(q)} &= \vec{\psi}^{(q)} + \frac{1}{2}\mu\left(\vec{\psi}^{(p)} - \vec{\psi}^{(q)}\right)\end{aligned} \tag{6}$$

where μ is the mixing extension which is a uniformly distributed random number with $\mu \in [0, 1]$. For this MCM mixing model, only N_{mix} times mixing processes take place, which is calculated as

$$N_{\text{mix}} = 3N_p C_\phi \omega_{\text{mix}} \mathrm{d}t \tag{7}$$

where C_ϕ is the mixing model parameter and dt the time marching step. From this equation, the ω_{mix} is the mixing frequency, a key physical parameter describing the mixing intensity. If ω_{mix} tends to be infinitely large, the PaSR model is identical to the PSR model since all the particles are perfectly mixed with each other. If ω_{mix} is too small, then the particles are hardly mixed with each other to support chemical reaction, and flame extinction can be observed [47, 48]. Therefore, the mixing process can have a significant impact on the chemical reaction process, and the predicted thermo-kinetic states are strongly dependent on the ω_{mix}.

To illustrate why the PaSR model is of great interest for the combustion system investigation, a numerical simulation has been performed by using the self-written PaSR4Comb package [51], and we give one example of averaged temperature against mixing frequency for the stoichiometric C_2H_4/air system under p=101.325 kPa in Fig. 5(a). Here, and throughout the whole work for the PaSR part, the ensemble-averaged values of thermo-kinetic state can be determined as

$$\langle\vec{\psi}\rangle = \frac{1}{N_p}\sum_{k=1}^{N_p}\vec{\psi}^{(k)} \tag{8}$$

It is observed here that with decreasing degree of mixing intensity (smaller mixing frequency), the averaged temperature decreases monotonically as well. This is consistent with the observation in Refs. [46, 48], in which more details and explanation can be found. However, it should be mentioned that at small mixing frequency, disparity between low-temperature and high-temperature particles becomes larger. Thus it is expected that more scatters can be observed at small mixing frequency, which is presented in Fig. 5(b).

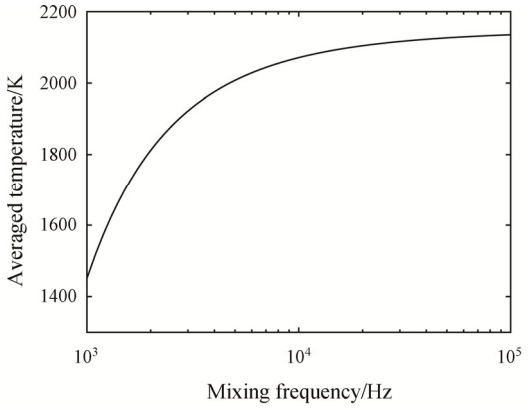

(a) Averaged temperature over mixing frequency

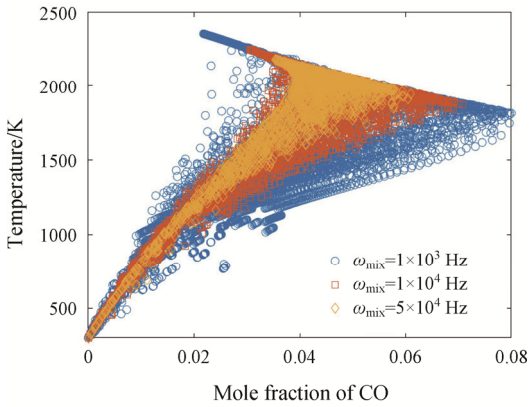

(b) Scatter plots: temperature and CO mole fraction

Fig. 5 Examples of (a) averaged temperature $\langle T\rangle$ over mixing frequency ω_{mix} and (b) scatter plots of temperature and mole fraction of CO based on detailed chemistry. Combustion system: Φ=1.0, p=101.325 kPa

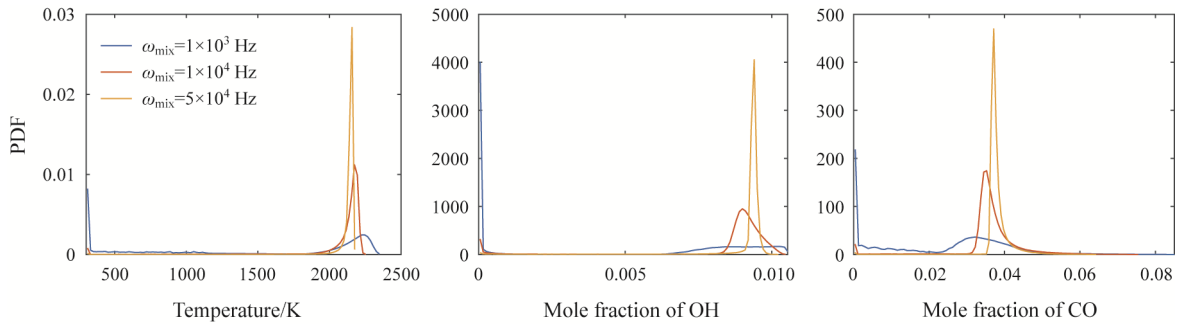

Fig. 6 Examples of PDFs for different quantities under three different mixing frequencies based on detailed chemistry. Combustion system: Φ=1.0, p=101.325 kPa

To evaluate the scatter, Fig. 6 shows the PDFs of temperature and mole fraction of OH and CO at three different mixing frequencies, from small mixing frequency (close to extinction limit) to large mixing frequency (close to PSR limit). These PDFs show that at high mixing frequency (here yellow lines), the thermo-kinetic states of all particles tend to be the same values and a peak PDF can be observed. In addition, due to high temperature at high mixing frequency (PSR limit), the chemical reaction for stoichiometric mixture also tends to be complete and CO is consumed to form CO_2. At small mixing frequency (here blue lines), the disparity between incoming cold particles and hot particles inside the reactor become large and two peaks of PDF can be observed.

This example shows that although the PaSR is a simple model, it provides a simple approach to analyze turbulence-chemistry interaction and its statistic behavior reflects the nature of turbulence. The skeletal mechanism needs also capture the statistic behavior at different mixing frequencies. Furthermore, with the consideration of extinction limits in the generation procedure, it is interesting to know whether the corresponding skeletal mechanism give better prediction for the statistic behavior.

3.2 Flame-flow interaction: spark ignition in strained premixed flame

The spark ignition process in a strained premixed flame can be considered as another configuration for flame-flow interaction. Depending on the flow velocity field (imposed by the strain rate in the flame), a flame kernel can be formed, leading to flame formation if sufficient spark energy is provided. In Refs. [52, 53], the spark ignition of laminar premixed flames in counterflow configuration is investigated, which is briefly outlined in the following together with Fig. 7.

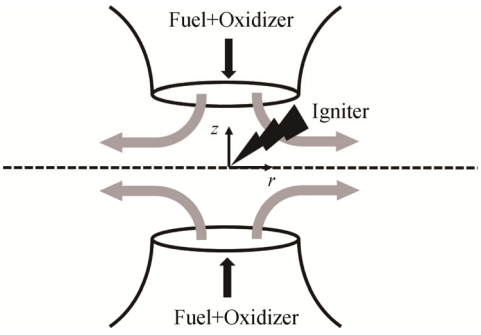

Fig. 7 Illustration of spark ignition model for strained premixed flame

The model is consistent with the one studied in Refs. [52, 53], and fuel and oxidizer with the same mixture composition is premixed in both inlets. A spark igniter is located at the stagnation point (z=0) to provide external energy to the system. The ignition can be successful and lead to development of a premixed flame, or the ignition can fail, depending on various model parameters.

The spark ignition energy is modelled using a prescribed spatio-temporal power density $\dot{q}_\mathrm{s}$ according to Ref. [54]:

$$\dot{q}_\mathrm{s}(z,t)=\begin{cases}\dfrac{D_\mathrm{s}}{\tau_\mathrm{s}}\cdot\exp\left[-\left(\dfrac{z}{\delta_\mathrm{w}}\right)^8\right] & \text{for } 0\le t\le\tau_\mathrm{s}\\ 0 & \text{otherwise}\end{cases} \tag{9}$$

Here, D_s is the maximum energy density (J/m^3) at z=0, and δ_w is the spark width. τ_s is the spark duration time describing how long the spark energy is provided into the system. Furthermore, the D_s can be determined by integrating the spark ignition energy over space and time as:

$$D_\mathrm{s}=\frac{\int_{z=-\infty}^{z=+\infty}\int_{t=0}^{\tau_\mathrm{s}}\dot{q}_s(z,t)\,\mathrm{d}t\mathrm{d}z}{2\cdot\delta_\mathrm{w}\cdot\Gamma\left(\dfrac{9}{8}\right)} \tag{10}$$

where $\Gamma(\cdot)$ is the gamma function ($\Gamma(9/8)\approx0.941\,74$).

The most important quantity for this validation case is the minimum energy for a successful spark ignition $D_\mathrm{s}^\mathrm{min}$, under which the combustion system cannot be successfully ignited and no steady burning flame can be obtained at the end.

This model has the advantage for validation due to the following two reasons:

(1) The effect of the flow parameter (namely the strain rate imposed in the flow) on the spark ignition can be accessed, and the skeletal mechanism should be able to capture this effect;

(2) As shown in Ref. [53], the sensitivity analysis showed that the most sensitive reactions for minimum ignition energy and ignition delay time are the same. Therefore, it is necessary to examine here whether the errors for $D_\mathrm{s}^\mathrm{min}$ caused by skeletal mechanisms remain in the same order of magnitude as the errors for ignition delay time.

3.3 Flame-wall interaction: Head-on Quenching (HoQ) process of laminar premixed flame

While above mentioned two validation models focus on the combustion system itself, the flame-wall interaction process provides the possibility to evaluate the quality of skeletal mechanism, if the combustion system is interacted with the solid wall where the heat loss from flame to wall must be considered. Besides some complex flame-wall interaction such as Side-Wall Quenching (SWQ) and Tube Quenching where at least two-dimensional numerical simulation is required

[55–58], the Head-on Quenching (HoQ) of unstrained laminar premixed flame is the most simple configuration to investigate the flame-wall interaction where one-dimensional numerical simulation is sufficient [59–62].

Fig. 8 displays the HoQ process of unstrained laminar premixed flame, where a flame front propagates perpendicular towards a cold wall (T_w). When the flame is close enough to the cold wall, heat loss from flame into the cold wall $\dot{q}_w$ increases which can be determined by using the Fourier's law:

$$\dot{q}_w = -\lambda\left(x=0^+\right)\cdot\left.\frac{\partial T}{\partial x}\right|_{x=0^{+'}} \tag{11}$$

where λ is the heat conductivity of unburnt gas mixture. Flame quenching takes place, if flame losses large amount of heat to the cold wall and the heat released by chemical reaction cannot support stable flame anymore. At the end, the temperature of flame decreases to the temperature the same as the cold wall.

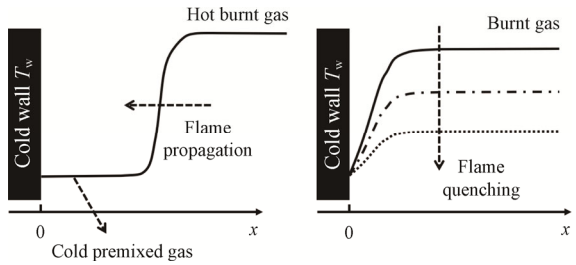

Fig. 8 Schematic illustration of Head-on Quenching (HoQ) process

A detailed numerical setup for the HoQ process throughout this work is consistent with the one described in our previous work [63]. As consistent with Refs. [61, 62, 64], for the HoQ process the flame quenching time is defined as the time when the heat loss to the cold wall (Eq. (11)) reaches its maximum, and the quenching distance d_q is defined as a distance between the cold wall and the location of the maximum of the global heat release rate (HRR). Typical spatial profiles of temperature and mole fractions of several selected species at the quenching time are shown in Fig. 9. It should be emphasized that there are different definitions for quenching distances [65, 66], which may lead to qualitatively different results. However, the main purpose of the present work is to validate the skeletal mechanism. Therefore, we select one possibility for the validation. It is expected that the conclusions and observations concerning the quality of skeletal mechanisms will not be affected by the definition of quenching distance.

The HoQ model provides the main advantage that the laminar flame speed and the quenching distance show the similar sensitive elementary reactions, as shown in Ref. [63]. Therefore, this model is useful to examine that if the skeletal mechanism is valid for laminar flame speed, whether it is also accurate for the prediction of quenching distance and the quenching process as well. Since the quenching distance is defined at the time point where the max. heat loss occurs, it is challenging for the skeletal mechanism that both the temperature gradient and the heat conductivity determined by the species concentration at the wall must be reproduced accurately.

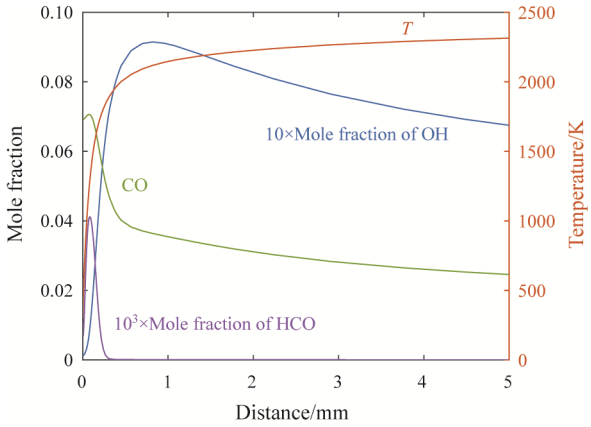

Fig. 9 Typical spatial profiles of temperature and mole fractions of different species at the quenching time

4. Results and Discussion

In the following, two STGSA-generated skeletal mechanisms, the sk-45sp and sk-33sp, are applied for above-mentioned three different premixed combustion configuration, and their accuracy is compared with the results by using the detailed chemistry. At the end of this part, the computational time will also be compared to illustrate the advantage of using skeletal mechanisms. It should be mentioned here again that the detailed chemistry includes 111 species.

4.1 Validation for PaSR model

In this part, we will focus on the validation of both skeletal mechanisms in the PaSR model to check, whether the dependence of different thermo-kinetic states on mixing frequency can be captured by skeletal mechanisms with good accuracy, and whether the statistics of the thermo-kinetic states (PDFs) can be well reproduced as well.

For the PaSR model, all incoming particles have the temperature of T=300 K, and the concentrations of species are identical to the concentration of unburnt C_2H_4/air mixture.

Fig. 10 shows the averaged temperature and averaged mole fraction of CO against mixing frequency predicted by detailed chemistry (symbols), sk-45sp (red) and sk-33sp (yellow) skeletal mechanisms for different

residence time. We notice that both skeletal mechanisms can give very good prediction, and the sk-33sp skeletal mechanism gives only slightly larger errors at low mixing frequencies.

Therefore, it seems that the quality of generated skeletal mechanisms is less sensitive at high mixing frequencies (in the near of PSR limit), but more sensitive at low mixing frequencies which are close to extinction (similar to the short residence time in PSR model, c.f. Fig. 3). This is because at low mixing frequencies, there is strong interaction between turbulence and chemistry, and thus the effect of mixing intensity on the chemistry must be taken into account. Furthermore, it is suggested to consider the extinction strain rate as a criterion in the generation of skeletal mechanisms. As discussed in Ref. [49], the mixing process is modeled using a mixing model to capture the correct scalar dissipation rate. Therefore, if the extinction strain rate, which is highly sensitive to molecular physical transport, can be accurately reproduced, then the scalar dissipation rate, even under high turbulence conditions, can also be well captured, resulting in higher accuracy for thermo-kinetic quantities.

Fig. 11 shows the statistic behaviors in terms of PDFs of mole fraction of CO under three different mixing frequencies and residence time. The mixing frequency and residence time for each subfigure is so selected, that the corresponding stochastic state is close to extinction state. Again the sk-45sp gives a very accurate prediction for PDFs, while the sk-33sp gives slightly deviation.

Fig. 12 shows further results on averaged temperature $\langle T \rangle$ (a) and averaged mole fraction of CO $\langle X(\mathrm{CO}) \rangle$ (b) over residence time τ_{res} for two different fuel/air equivalence ratios. We observe here that for both cases, the sk-45sp results agree with the detailed results very good, while the sk-33sp results have noticeable deviations, especially for the case with fuel/air equivalence ratios Φ=1.6. Even for Φ=0.6, the deviation at low mixing frequencies can be observed.

From these observations, we can conclude that:

(1) at high mixing frequencies, the skeletal mechanism generated by considering and validating only the ignition delay time and laminar flame speed is accurate enough to predict the averaged thermo-kinetic states and statistic behaviors.

(2) at low mixing frequencies, especially close to extinction, the consideration of strain rate on the generation of skeletal mechanism is suggested to reproduce a better prediction for averaged thermo-kinetic states and statistic behaviors.

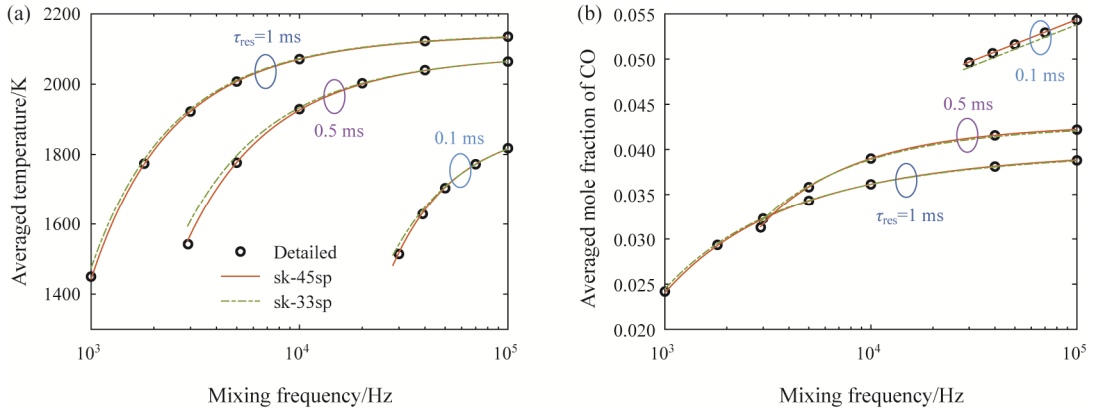

Fig. 10 Averaged temperature $\langle T \rangle$ (a) and averaged mole fraction of CO $\langle X(\mathrm{CO}) \rangle$ (b) over mixing frequency ω_{mix}. Combustion system: Φ=1.0, p=101.325 kPa

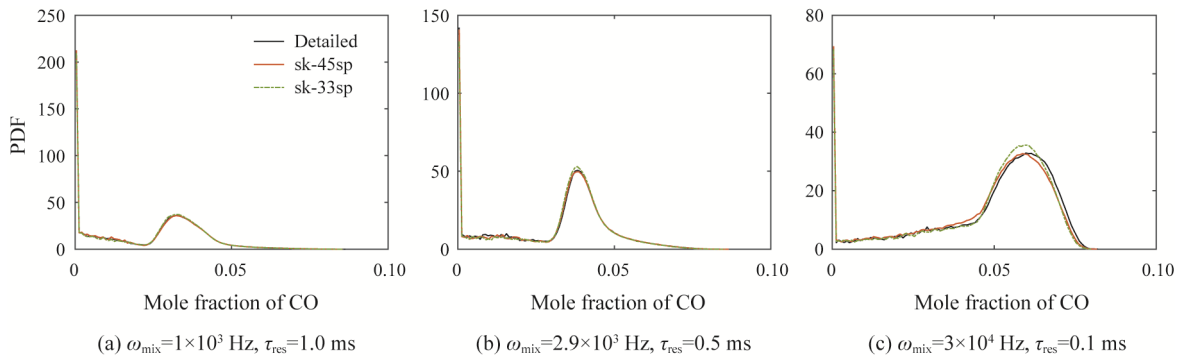

Fig. 11 Statistic behaviors in terms of PDFs of mole fraction of CO under three different mixing frequencies and residence time

4.2 Validation for spark ignition

For the validation of spark ignition process, we consider here the premixed gas mixture with fuel/air equivalence ratio Φ=0.6 as a candidate. The spark width δ_w=1 mm and the spark duration time τ_s=1 ms are selected. It should be mentioned that the conclusion in this part also holds for other model parameters.

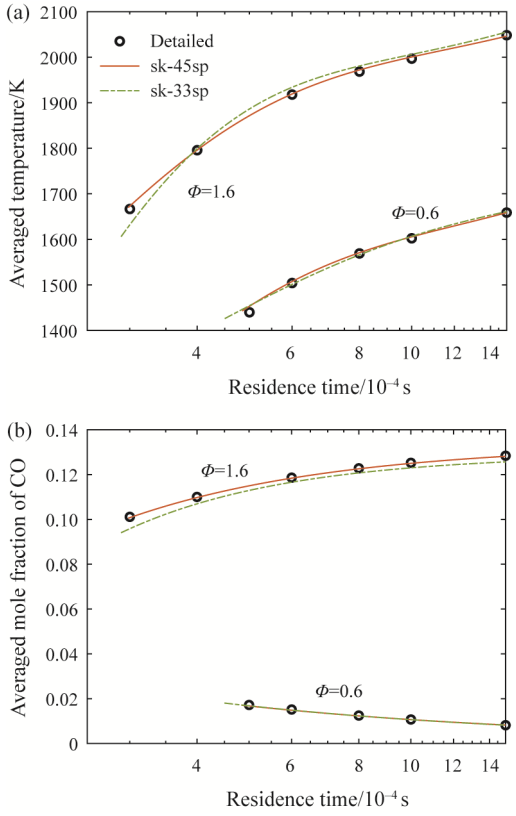

Fig. 12 Averaged temperature $\langle T \rangle$ (a) and averaged mole fraction of CO $\langle X(\mathrm{CO}) \rangle$ (b) over residence time τ_{res}. Combustion system: p=101.325 kPa.

In Fig. 13, we shows that comparison of two skeletal mechanisms for the prediction of minimum energy for a successful spark ignition under different strain rates. It shows clearly that although the sk-45sp gives better accuracy, the sk-33sp, which is generated by only considering the IDT, gives also very good prediction with max. error less than 1.5%.

This result shows clearly that if the skeletal mechanism is accurate for the prediction of ignition delay time, it is also accurate for the prediction of minimum ignition energy, and the increase of minimum ignition energy with increasing strain rate can also be captured very well. This is because, as explained in Ref. [53], whether a gas mixture can be successfully ignited or not largely depends on the reaction rate right after the spark duration time, which can be characterized by the inverse of IDT.

4.3 Validation for HoQ process

In this part, we will focus on validating the transient HoQ process, especially the prediction for quenching distance d_q, as shown in Fig. 14. We notice that the errors for d_q caused by two skeletal mechanisms remain almost the same as those for laminar flame speed (c.f. Fig. 2), namely the errors caused by sk-45sp are less than 2%, and the errors caused by sk-33sp are mostly 4%–7%.

Fig. 15 further shows the mole fraction of CO at wall, since it is the main emission at cold wall during the transient quenching process [67, 68]. It shows clearly that the CO concentration at the wall can be very well predicted by using both skeletal mechanisms, and the max. error is caused by sk-33sp with around 4%. The main reason is that in the generation of STGSA skeletal mechanism, CO shows the 8th most important species for global sensitivity. This means that the CO species plays an important role in the prediction of IDT, and all reactions associated with CO species are kept in the

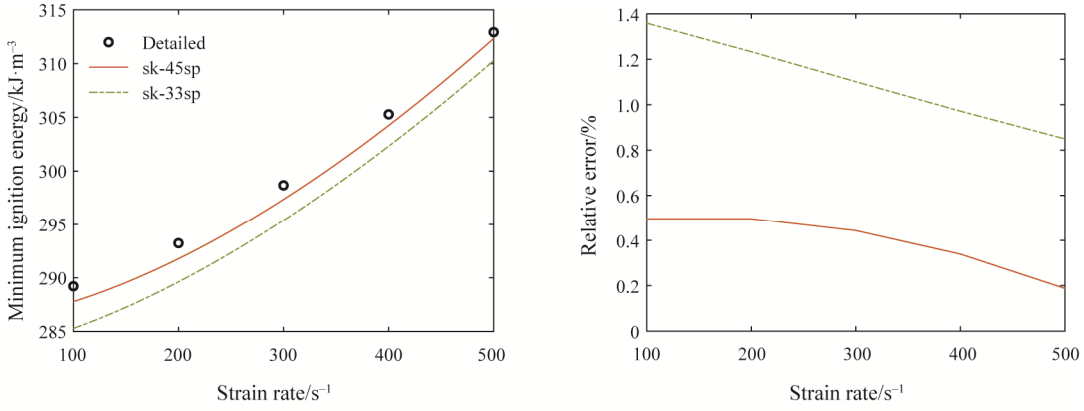

(a) Comparison of minimum ignition energy (b) Relative errors of two skeletal mechanisms

Fig. 13 Circles: detailed mechanism (circles); Solid lines: sk-45sp, the 45-species skeletal mechanism; Dashed lines: sk-33sp, the 33-species skeletal mechanism. Φ=0.6. The unburnt gas temperature: 300 K; Pressure: 101.325 kPa.

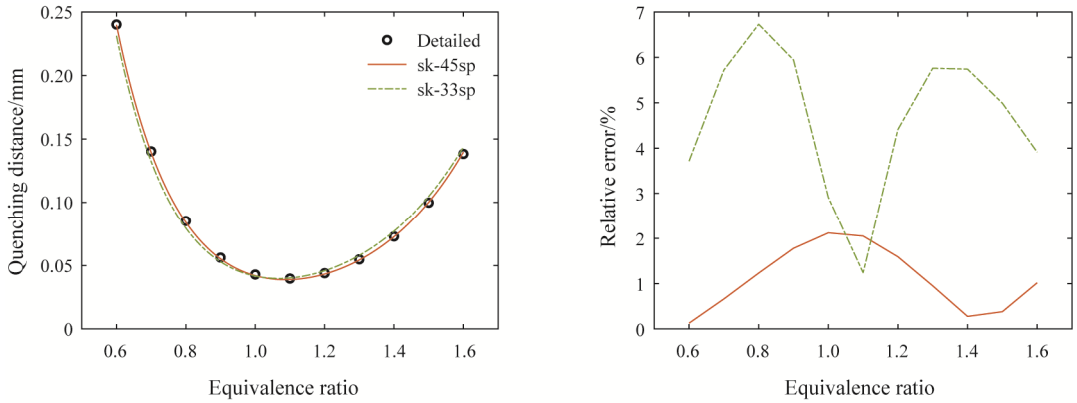

(a) Comparison of quenching distance (b) Relative errors of two skeletal mechanisms

Fig. 14 Circles: detailed mechanism (circles); Solid lines: sk-45sp, the 45-species skeletal mechanism; Dashed lines: sk-33sp, the 33-species skeletal mechanism. The unburnt gas temperature: 300 K; Pressure: 101.325 kPa.

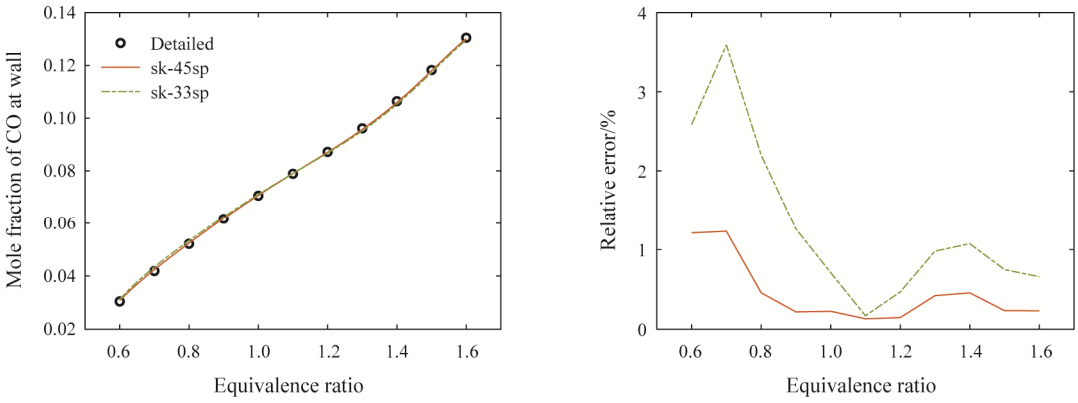

(a) Comparison of CO mole fraction at wall (b) Relative errors of two skeletal mechanisms

Fig. 15 Circles: detailed mechanism (circles); Solid lines: sk-45sp, the 45-species skeletal mechanism; Dashed lines: sk-33sp, the 33-species skeletal mechanism. The unburnt gas temperature: 300 K; Pressure: 101.325 kPa.

skeletal mechanisms. Therefore, the CO concentration can be predicted in a high accuracy.

Further results in Fig. 16 compares the spatial profiles of temperature and mole fraction of CO at the time of quenching (max. heat loss at the wall) for three different fuel/air equivalence ratios. We notice that there are almost no evident differences for temperature profile, and small disparity for the mole fraction of CO profiles is only observed by using the sk-33sp. The results by using sk-45sp give almost identical results as by using detailed chemistry.

These results show clearly that if the skeletal mechanism is validated for the ignition delay time and laminar flame speeds, it is also valid for the application in transient flame-wall interaction. Those species, which give high sensitivity indices and are kept in the STGSA generated skeletal mechanism, can also be well predicted.

4.4 Computational time

In the last part, the computational time by using detailed chemistry and two skeletal mechanisms are compared. The relative CPU time is defined in the way that the averaged computational time is normalized by the computational time using the detailed chemistry. Fig. 17 shows the comparison for three considered combustion validation models:

(1) For both PaSR model and HoQ process, the sk-45sp mechanism uses only 20% CPU time compared to the CPU time used by detailed chemistry, and the sk-33sp mechanism uses even less CPU time.

(2) For spark ignition model, the CPU time used by sk-45sp is around 40% of the CPU time used by detailed chemistry, which is not significant compared to other two cases. This phenomenon can be attributed to the following reason: during spark deposition, the mixture is heated up without chemical reaction. Therefore, the governing equations for energy and species are solved with the source term approximated to zero. After the spark igniter is removed, the mixture with high temperature will further self-ignite or extinguish. The self-ignition process runs much faster (on the order of the ignition delay time) than the physical transport process.

Therefore, within a very short time, we can observe the formation of a flame kernel and determine whether it is a case of successful spark ignition or failed spark ignition. If one is interested in the entire transient spark ignition process until a steady flame is established, then using a skeletal mechanism is expected to save more CPU time.

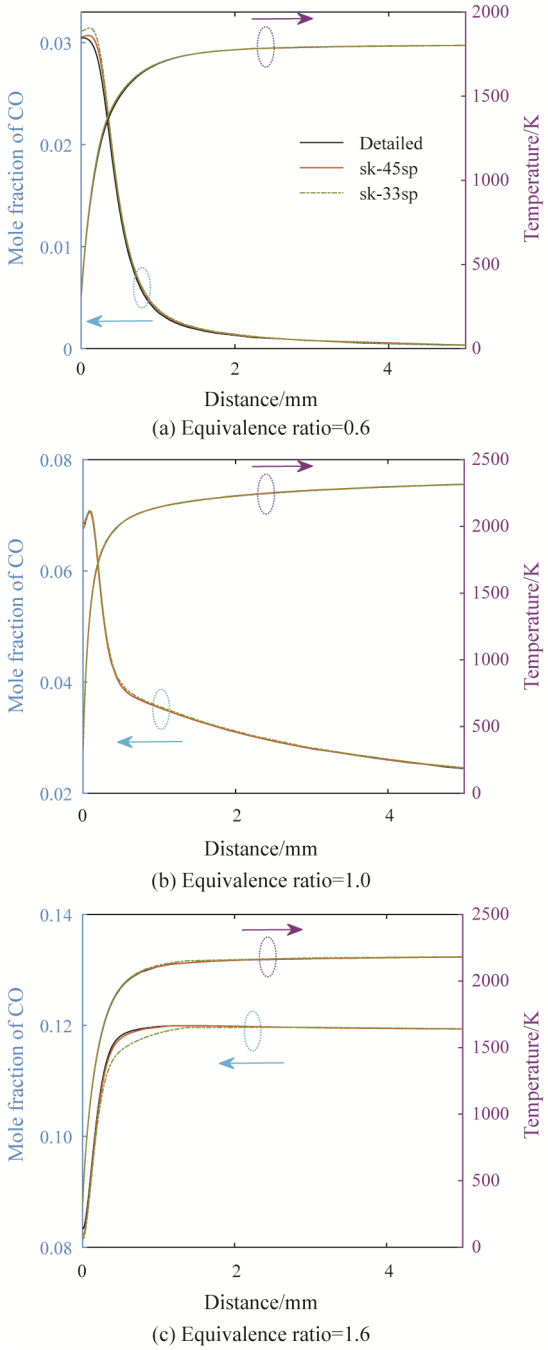

Fig. 16 Spatial distribution of temperature and mole fraction of CO at quenching time based on detailed chemistry (black), sk-45sp skeletal mechanism (red) and sk-33sp skeletal mechanism (green).

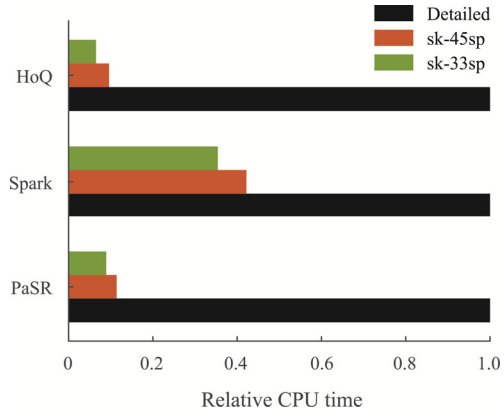

Fig. 17 Comparison of relative computational (CPU) time for three different validation models

5. Conclusions

In this study, a comprehensive assessment has been performed for the STGSA- generated skeletal mechanism for C_2H_4/air. Two different STGSA-reduced mechanisms are applied incorporating foundational combustion models such as the homogeneous reactor model, one-dimensional flat premixed flame, and non-premixed counterflow flame. Subsequently, these reduced mechanisms are applied to more complex combustion scenarios, taking into consideration additional physical parameters and intricate processes. Namely flame-flow interaction and flame-wall interaction.

The outcomes of our investigation demonstrate the capability of the skeletal mechanism to adeptly capture the flame behaviors in these complex combustion systems. The quenching process and the spark ignition process (in terms of minimum ignition energy) can be well captured by the skeletal mechanisms generated by considering only the ignition delay time as validation quantity. However, for the turbulence-chemistry interaction process, if the turbulent intensity becomes larger, the inclusion of strain rate considerations in generating the skeletal mechanism is suggested to capture the stochastic steady state and the statistic behaviors better.

In ongoing research, it is valuable to identify the dominant reactions and species for different cases not only globally (as used in STGSA) but also locally. This may aid in enhancing the algorithm for generating the skeletal mechanism by considering more efficient target quantities.

Acknowledgements

Work done by C. YU is supported by the Shanghai Science and Technology Program within the project “Research of combustion reaction kinetics of a

multi-component e-fuel for efficient utilization" (Grant No. 23160711900).

Conflict of Interest

YANG Bin is an editorial board member for Journal of Thermal Science and was not involved in the editorial review or the decision to publish this article. All authors declare that there are no competing interests.

Funding note

Open Access funding enabled and organized by Projekt DEAL.

References

[1] Goussis D.A., Maas U., Model reduction for combustion chemistry. In: Turbulent Combustion Modeling: Advances, New Trends and Perspectives, Springer, Dordrecht, 2011, pp. 193–220.

[2] Turányi T., Tomlin A.S., Analysis of kinetic reaction mechanisms. Springer, Berlin Heidelberg, 2014.

[3] Gorban A.N., Model reduction in chemical dynamics: slow invariant manifolds, singular perturbations, thermodynamic estimates, and analysis of reaction graph. Current Opinion in Chemical Engineering, 2018, 21: 48–59.

[4] Ren Z., Pope S.B., The use of slow manifolds in reactive flows. Combustion and Flame, 2006, 147(4): 243–261.

[5] Zhang P., Zsély I.G., Papp M., Nagy T., Tur´anyi T., Comparison of methane combustion mechanisms using laminar burning velocity measurements. Combustion and Flame, 2022, 238: 111867.

[6] Chi C., Thévenin D., DNS study on reactivity stratification with prechamber H_2/air turbulent jet flame to enhance NH_3/air combustion in gas engines. Fuel, 2023, 347: 128387.

[7] Xin Y.X., Yoo C.S., Chen J.H., Law C.K., A DNS study of self-accelerating cylindrical hydrogen-air flames with detailed chemistry. Proceedings of the Combustion Institute, 2015, 35(1): 753–760.

[8] Lai J., Klein M., Chakraborty N., Direct numerical simulation of head-on quenching of statistically planar turbulent premixed methane-air flames using a detailed chemical mechanism. Flow, Turbulence and Combustion 2018, 101: 1073–1091.

[9] Cleary M., Klimenko A., Janicka J., Pfitzner M., A sparse-lagrangian multiple mapping conditioning model for turbulent diffusion flames. Proceedings of the Combustion Institute, 2009, 32(1): 1499–1507.

[10] Navarro-Martinez S., Kronenburg A., LES-CMC simulations of a lifted methane flame. Proceedings of the Combustion Institute, 2009, 32(1): 1509–1516.

[11] Minamoto Y., Chen J.H., DNS of a turbulent lifted DME jet flame. Combustion and Flame, 2016, 169: 38–50.

[12] Zettervall N., Nordin-Bates K., Nilsson E., Fureby C., Large eddy simulation of a premixed bluff body stabilized flame using global and skeletal reaction mechanisms. Combustion and Flame, 2017, 179: 1–22.

[13] Zettervall N., Fureby C., Nilsson E., A reduced chemical kinetic reaction mechanism for kerosene-air combustion. Fuel, 2020, 269: 117446.

[14] Wei X., Wang J., Zhang M., Huang Z., Large eddy simulation study on the turbulence and flame characteristics under analogical integral scale and turbulence intensity of turbulent premixed flames. Journal of Thermal Science, 2023, 32(1): 488–501.

[15] Wang F., Wang Y., Wei G., Liu D., Jin J., Jones W.P., Flame structure of methane and kerosene combustion with a compact concave flame-holder using the LES-PDF method. Journal of Thermal Science, 2024, 33(1): 222–234.

[16] Maas U., Pope S.B., Simplifying chemical kinetics: intrinsic low-dimensional manifolds in composition space. Combustion and Flame, 1992, 88(3–4): 239–264.

[17] Peters N., Laminar diffusion flamelet models in non-premixed turbulent combustion. Progress in Energy and Combustion Science, 1984, 10(3): 319–339.

[18] Pitsch H., Ihme M., An unsteady/flamelet progress variable method for les of nonpremixed turbulent combustion. In: 43rd AIAA Aerospace Sciences Meeting and Exhibit, 2005, AIAA-557.

[19] Fiorina B., Baron R., Gicquel O., Thevenin D., Carpentier S., Darabiha N., Modelling non-adiabatic partially premixed flames using flame-prolongation of ILDM. Combustion Theory and Modelling, 2003, 7(3): 449.

[20] Bykov V., Maas U., The extension of the ILDM concept to reaction-diffusion manifolds. Combustion Theory and Modelling, 2007, 11(6): 839–862.

[21] Jones W., Lindstedt R., Global reaction schemes for hydrocarbon combustion. Combustion and Flame, 1988, 73(3): 233–249.

[22] Maio G., Cailler M., Mercier R., Fiorina B., Virtual chemistry for temperature and co prediction in les of non-adiabatic turbulent flames. Proceedings of the Combustion Institute, 2019, 37(2): 2591–2599.

[23] Lam S.-H., Goussis D.A., Understanding complex chemical kinetics with computational singular perturbation. Symposium (International) on Combustion, 1989, 22: 931–941.

[24] Lu T., Law C.K., A directed relation graph method for mechanism reduction. Proceedings of the Combustion

Institute, 2005, 30(1): 1333–1341.

[25] Niemeyer K.E., Sung C.-J., Raju M.P., Skeletal mechanism generation for surrogate fuels using directed relation graph with error propagation and sensitivity analysis. Combustion and Flame, 2010, 157(9): 1760–1770.

[26] Minuzzi F., Pinho J.M., A new skeletal mechanism for ethanol using a modified implementation methodology based on directed relation graph (DRG) technique. Journal of the Brazilian Society of Mechanical Sciences and Engineering, 2020, 42: 1–14.

[27] Pepiot-Desjardins P., Pitsch H., An efficient error-propagation-based reduction method for large chemical kinetic mechanisms. Combustion and Flame, 2008, 154(1–2): 67–81.

[28] Stagni A., Frassoldati A., Cuoci A., Faravelli T., Ranzi E., Skeletal mechanism reduction through species-targeted sensitivity analysis. Combustion and Flame, 2016, 163: 382–393.

[29] Bhagatwala A., Luo Z., Shen H., Sutton J.A., Lu T., Chen J.H., Numerical and experimental investigation of turbulent DME jet flames. Proceedings of the Combustion Institute, 2015, 35(2): 1157–1166.

[30] Lu T., Law C.K., Strategies for mechanism reduction for large hydrocarbons: n-heptane. Combustion and Flame, 2008, 154(1–2): 153–163.

[31] Luca S., Al-Khateeb A.N., Attili A., Bisetti F., Comprehensive validation of skeletal mechanism for turbulent premixed methane-air flame simulations. Journal of Propulsion and Power, 2018, 34(1): 153–160.

[32] Chen Z., Vom Lehn F., Pitsch H., Cai L., Prediction of sooting index of fuel compounds for spark-ignition engine applications based on a machine learning approach. Journal of Thermal Science, 2023, 32(2): 521–530.

[33] Wang C., Yue Z., Zhao Y., Ye Y., Liu X., Liu H., Numerical simulation of the high-boosting influence on mixing, combustion and emissions of high-power-density engine. Journal of Thermal Science, 2023, 32(3): 933–946.

[34] Lin S., Xie M., Wang J., Liang W., Law C.K., Zhou W., Yang B., Chemical kinetic model reduction through species-targeted global sensitivity analysis (STGSA). Combustion and Flame, 2021, 224: 73–82.

[35] Eckart S., Yu C., Lin S., Maas U., Krause H., Yang B., An experimental and modeling study on extinction strain rate and laminar burning velocity in C_2H_x flames. under review.

[36] Chen Z., Reddy V., Ruan S., Doan N., Roberts W.L., Swaminathan N., Simulation of mild combustion using perfectly stirred reactor model. Proceedings of the Combustion Institute, 2017, 36(3): 4279–4286.

[37] Chen J.-Y., Dibble R.W., A perfectly-stirred-reaction description of chemistry in turbulent nonpremixed combustion of methane in air. Combustion Science and Technology, 1992, 84(1–6): 45–50.

[38] Hao N.T., A chemical reactor network for oxides of nitrogen emission prediction in gas turbine combustor. Journal of Thermal Science, 2014, 23: 279–284.

[39] Zhu Z., Xiong Y., Liu Z., Zhang Z., Effect of steam dilution on the mild combustion characteristics of methane in a model combustor. Journal of Thermal Science, 2023, 32(2): 822–836.

[40] Glarborg P., Kee R.J., Grcar J.F., Miller J.A., PSR: A FORTRAN program for modeling well-stirred reactors. Sandia National Laboratories Livermore, California, 1986.

[41] Snegirev A.Y., Perfectly stirred reactor model to evaluate extinction of diffusion flame. Combustion and Flame, 2015, 162(10): 3622–3631.

[42] Shan R., Lu T., Ignition and extinction in perfectly stirred reactors with detailed chemistry. Combustion and Flame 2012, 159(6): 2069–2076.

[43] Sun W., Chen Z., Gou X., Ju Y., A path flux analysis method for the reduction of detailed chemical kinetic mechanisms. Combustion and Flame, 2010, 157(7): 1298–1307.

[44] Si J., Wang G., Li P., Mi J., A new skeletal mechanism for simulating mild combustion optimized using artificial neural network. Energy, 2021, 237: 121603.

[45] Prieler R., Mayr B., Viehböck D., Demuth M., Hochenauer C., Sensitivity analysis of skeletal reaction mechanisms for use in CFD simulation of oxygen enhanced combustion systems. Journal of the Energy Institute, 2018, 91(3): 369–388.

[46] Chen J.-Y., Stochastic modeling of partially stirred reactors. Combustion Science and Technology, 1997, 122(1–6): 63–94.

[47] Correa S.M., Turbulence-chemistry interactions in the intermediate regime of premixed combustion. Combustion and Flame, 1993, 93(1–2): 41–60.

[48] Yu C., Cai L., Chen J.-Y., Stochastic modeling of partially stirred reactor (PASR) for the investigation of the turbulence-chemistry interaction for the ammonia-air combustion. Flow, Turbulence and Combustion, 2024, 112: 509–536.

[49] Pope S.B., PDF methods for turbulent reactive flows. Progress in Energy and Combustion Science, 1985, 11(2): 119–192.

[50] Janicka J., Kolbe W., Kollmann W., Closure of the transport equation for the probability density function of turbulent scalar fields. Journal of Non-Equilibrium Thermodynamics, 1979, 4: 47–66.

[51] Yu C., Matlab-based PaSR-PDF code.

https://github.com/ChunkanYu/Stochastic-Modeling-PaSR-for-Combustion, 2023.

[52] Yu C., Eckart S., Essmann S., Markus D., Valera-Medina A., Schießl R., Shu B., Krause H., Maas U., Investigation of spark ignition processes of laminar strained premixed stoichiometric NH_3-H_2-air flames. Journal of Loss Prevention in the Process Industries, 2023, 83: 105043.

[53] Yu C., Markus D., Schießl R., Maas U., Numerical study on spark ignition of laminar lean premixed methane-air flames in counterflow configuration. Combustion Science and Technology, 2023, 195(9): 2085–2109.

[54] Maas U., Raffel B., Wolfrum J., Warnatz J., Observation and simulation of laser induced ignition processes in O_2-O_3 and H_2-O_2 mixtures. Symposium (International) on Combustion, 1988, 21(1): 1869–1876.

[55] Luo M., Ren H., Chen C., Liu D., Soot formation in asymmetrical ethylene jet flame-wall interactions. Journal of the Energy Institute, 2023, 106: 101157.

[56] Bai B., Chen Z., Zhang H., Chen S., Flame propagation in a tube with wall quenching of radicals. Combustion and Flame, 2013, 160(12): 2810–2819.

[57] Zirwes T., Häber T., Zhang F., et al., Numerical study of quenching distances for side-wall quenching using detailed diffusion and chemistry. Flow, Turbulence and Combustion, 2021, 106: 649–679.

[58] Luo G., Dai H., Dai L., Qian Y., Sha C., Zhang Y., Wu B., Review on large eddy simulation of turbulent premixed combustion in tubes. Journal of Thermal Science, 2020, 29(4): 853–867.

[59] Poinsot T., Veynante D., Theoretical and numerical combustion. RT Edwards, Inc., Philadeplhia, USA, 2005.

[60] Wichman I.S., Bruneaux G., Head-on quenching of a premixed flame by a cold wall. Combustion and Flame, 1995, 103(4): 296–310.

[61] Westbrook C.K., Adamczyk A.A., Lavoie G.A., A numerical study of laminar flame wall quenching. Combustion and Flame, 1981, 40: 81–99.

[62] Popp P., Baum M., Analysis of wall heat fluxes, reaction mechanisms, and unburnt hydrocarbons during the head-on quenching of a laminar methane flame. Combustion and Flame, 1997, 108(3): 327–348.

[63] Yu C., Cai L., Chi C., Mashruk S., Valera-Medina A., Maas U., Numerical investigation on the head-on quenching (HoQ) of laminar premixed lean to stoichiometric ammonia-hydrogen-air flames. Flow, Turbulence and Combustion, 2023, 111: 1301–1322.

[64] Sotton J., Boust B., Labuda S., Bellenoue M., Head-on quenching of transient laminar flame: heat flux and quenching distance measurements. Combustion Science and Technology, 2005, 177(7): 1305–1322.

[65] Dabireau F., Cuenot B., Vermorel O., Poinsot T., Interaction of flames of H_2+O_2 with inert walls. Combustion and Flame, 2003, 135(1–2): 123–133.

[66] Li H., Interaction of end-gas autoignition and cold wall in closed chamber. Combustion and Flame, 2024, 259: 113158.

[67] Palulli R., Talei M., Gordon R.L., Unsteady flame-wall interaction: Impact on co emission and wall heat flux. Combustion and Flame, 2019, 207: 406–416.

[68] Li F., Pan J., Zhu Y., Li Z., Zhu J., Nauman M., Effect of hydrogen addition on co emission and thermo-chemical state near wall during head-on quenching of laminar premixed methane/air flame. International Journal of Hydrogen Energy, 2024, 49: 1425–1436.